Anti-Hermitian Plasmon Coupling of an Array of Gold Thin-Film Antennas for Controlling Light at the Nanoscale

Shuang Zhang,[1,2] Ziliang Ye,[1] Yuan Wang,[1] Yongshik Park,[1] Guy Bartal,[1] Michael Mrejen,[1] Xiaobo Yin,[3] and Xiang Zhang[1,3,*]

[1]*Nanoscale Science and Engineering Center, 5130 Etcheverry Hall, University of California, Berkeley, California 94720-1740, USA*
[2]*School of Physics and Astronomy, University of Birmingham, Birmingham, B15 2TT, United Kingdom*
[3]*Materials Sciences Division, Lawrence Berkeley National Laboratory, 1 Cyclotron Road Berkeley, California 94720, USA*

(Received 2 April 2012; published 9 November 2012; corrected 6 December 2012)

Open quantum systems consisting of coupled bound and continuum states have been studied in a variety of physical systems, particularly within the scope of nuclear, atomic, and molecular physics. In the open systems, the effects of the continuum decay channels are accounted for by indirect non-Hermitian couplings among the quasibound states. Here we explore anti-Hermitian coupling in a plasmonic system for spatially manipulating light on the nanoscale. We show that by utilizing the anti-Hermitian coupling, plasmonic antennas closely packed within only $\lambda/15$ separations can be individually excited from the far field, which are otherwise indistinguishable from each other. This opens a new venue for the nanoscale lightwave control, wavelength multiplexing, and spectrum splitting.

DOI: 10.1103/PhysRevLett.109.193902 PACS numbers: 42.25.Bs, 78.20.Ci, 78.67.Pt

The indirect coupling among quasibound states through common continuum decay channels has been widely studied in various open quantum systems, in particular, for the investigation of the resonance phenomena in nuclei, atoms, molecules, and quantum dots [1–3]. Interesting features of these systems have been observed, such as the restructuring of the eigenstates with contrasting lifetimes in the system: some long-lived states are deprived of the coupling strength to the decay channels, while others with enhanced coupling to the decay channels having very short lifetime, i.e., the so-called "superradiant" states that were first proposed by Dicke for describing the coherent spontaneous radiation of a gas confined to a subwavelength scale [4]. Spectroscopically, this phenomenon is manifested as sharp resonances superimposed on the broad superradiant states, as observed, for example, in the decay of compound nuclear states in certain nuclear reactions [5–7].

A general treatment of the open systems, the standard projection formalism, divides the Hilbert space of an open system into two subspaces, the $\{\mathcal{Q}\}$ subspace that consists of interior quasibound (discrete) states $|q\rangle$ and the $\{P\}$ subspace that only consists of the continuum decay channels $|c\rangle$, with $\mathcal{Q}$ and P being the projection operators of the two subspaces [8]. The effective Hamiltonian acting on the bound states by taking into account the indirect coupling mediated by the continuum decay channels can be written as [9]

$$H_{\text{eff}} = H_{\mathcal{Q}\mathcal{Q}} + H_{\mathcal{Q}P}(E - H_{PP})^{-1}H_{P\mathcal{Q}}, \tag{1}$$

where $H_{\mathcal{Q}\mathcal{Q}}$ is the Hamiltonian projected in the subspace of quasibound states, $H_{\mathcal{Q}P}$ and $H_{P\mathcal{Q}}$ are the coupling matrices between the $\mathcal{Q}$ and P subspaces, and $(E - H_{PP})^{-1}$ is the propagator in the subspace of open channels. The second term on the right-hand side (rhs) of Eq. (1) represents the indirect interaction among the bound states mediated by the open (continuum) channels. The matrix elements of the effective Hamiltonian can be further expressed as [1]

$$\langle q_1|H_{\text{eff}}|q_2\rangle = \langle q_1|H_{\mathcal{Q}\mathcal{Q}}|q_2\rangle + \sum_{c=1}^{K} \text{P.V.} \int dE' \frac{V_{q_1}^c V_{q_2}^c}{E - E'} - \frac{i}{2}\sum_{c=1}^{K} V_{q_1}^c V_{q_2}^c,$$

or in the matrix form

$$H_{\text{eff}} = H_{\mathcal{Q}\mathcal{Q}} + \text{P.V.} \int dE \frac{VV^+}{E - E'} - \frac{i}{2}VV^+, \tag{2}$$

where P.V. denotes the Cauchy principal value of the integral, $V_q^c = \sqrt{2\pi}\langle q|H_{\mathcal{Q}P}|c\rangle$, and K is the number of decay channels. Thus, within the quasibound states subspace, the effective Hamiltonian of the system contains an imaginary, or anti-Hermitian coupling matrix $(-iVV^+/2)$ that arises from the indirect coupling among the bound states mediated by the open channels [10,11]. For an open quantum system consisting of M bound states coupled to K continuum decay channels, the coupling matrix V between the discrete and continuum subspaces is of dimension $M \times K$, and the indirect anti-Hermitian coupling matrix $-iVV^+/2$ has a dimension of $M \times M$, but with a rank of K in the case of $M > K$. For an open system with a single common decay channel $(K = 1)$, $V = [V_1, V_2, \ldots, V_p, \ldots]^T$ is simply a column vector. Note that the Cauchy principal value of the indirect coupling [second term on the rhs of Eq. (2)], which is real and generally nonzero, leads to a shift of the energies of eigenstates, which corresponds to the so-called collective Lamb shift [9,12–14].

The governing Hamilitonian for a quantum open system with a single continuum channel can be mapped to a

plasmonic system consisting of an array of plasmonic dipole antennas with the same orientation positioned in proximity to each other (separations < wavelength). The mutual couplings among plasmonic resonators offer great flexibility in tailoring their optical properties, such as tuning the resonance frequency and controlling the line shape of resonance [15–22]. Being an open system, the coupling can generally be divided into two parts, the direct near-field coupling and the indirect coupling mediated by radiative channels, i.e., continuum states. For antennas with small separations and the same orientation, the antennas primarily couple to the same dipolar radiation mode, i.e., a single decay channel with $K = 1$. In addition, the separations between the antennas can be carefully designed so that the effect of the direct near-field coupling and the Cauchy principal value of the indirect coupling counteract each other, and the system is dominated by the anti-Hermitian part of the indirect coupling.

Recently, there have been explorations of electromagnetically induced absorption, or superscattering in plasmonic systems, which show optical effects opposite to the well-studied plasmon induced transparency [23,24]. In those systems, the anti-Hermitian coupling plays an important role for introducing a constructive interference among different excitation pathways to enhance the scattering [25,26]. In this work, we show that continuum mediated anti-Hermitian coupling in an array of densely positioned plasmonic antennas can be utilized for spatially manipulating light in the deep subwavelength scale. We consider an array of plasmonic antennas with different resonance frequencies $\omega_i \neq \omega_j$ and investigate the coupling phenomena of antennas under the excitation of a plane wave. The general form of the coupled equations can be written as

$$\sum_q [(-\omega + \omega_p - i\gamma_p)\delta_{pq} - (1 - \delta_{pq})\kappa_{pq}]A_q = g_p E_0, \tag{3}$$

where γ_p is the dissipation term, κ_{pq} ($\kappa_{pq} = \kappa_{qp}$) is the coupling coefficient between the pth and qth antennas, g_p denotes the coupling strength between the incident plane wave and the antenna, with $g_p \propto V_p$, and E_0 is the electric field of the incident wave. For dipole antennas operating at infrared frequencies, the overall loss is usually dominated by the radiation loss (coupling to the continuum channel). For simplicity of analysis, we assume that γ_p only contains the radiation loss. We further assume an ideal case that the Hermitian part of the overall coupling, which includes the direct near-field coupling and the Cauchy principal value of the indirect coupling, vanishes, and κ_{pq} only consists of the indirect coupling mediated by the single decay channel. With the above assumptions, $i\gamma_p$ and κ_{pq} are just the diagonal and off-diagonal elements of the anti-Hermitian coupling tensor $iVV^+/2$, respectively; i.e.,

$$i\gamma_p = iV_p^2/2, \qquad \kappa_{pq} = iV_pV_q/2. \tag{4}$$

At the resonance frequency of the pth antenna ($\omega = \omega_p$), Eq. (3) can be solved as

$$A_p = \frac{2ig_p}{V_p^2}, \qquad A_q(q \neq p) = 0. \tag{5}$$

Equation (5) suggests that only a single resonator can be selectively excited at its resonance frequency, whereas all the others remain completely unexcited. In a strongly coupled system the eigenstates of the multiantenna system are hybridized excitations of more than one resonator. This indicates that, under plane wave excitation of the antenna array, multiple eigenstates are simultaneously excited, which interfere constructively at a single resonator and destructively at all the others, leading to a highly localized state. Since the spatial separation between the neighboring antennas can be much less than the wavelength of the incident electromagnetic wave, the plasmonic system governed by anti-Hermitian coupling offers an interesting platform for manipulation of light in the deep subwavelength scale.

A simple implementation of a plasmonic system exhibiting anti-Hermitian indirect coupling mediated by a single open channel is shown in Fig. 1. The system consists of two optical dipole antennas [27] of slightly different lengths with deep subwavelength spacing [Fig. 1(a)]. Each optical antenna is capable of focusing light into the gap region of nanometer scales. Numerical simulation (CST MICROWAVE STUDIO) was carried out to calculate the optical response of each antenna at their gap centers under the illumination of a plane wave at normal incidence, and numerical fitting was subsequently employed to retrieve the coupling constant between the two antennas [28].

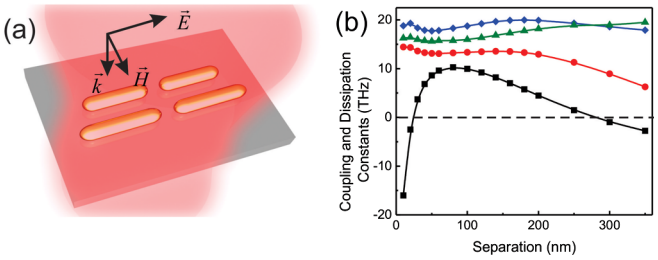

FIG. 1 (color online). Numerical retrieval of the indirect anti-Hermitian coupling between two optical antennas. (a) A plasmonic system consisting of two optical antennas made of gold on a quartz substrate. The lengths of the antennas are 430 and 470 nm. The width and thickness of both antennas are 40 and 25 nm, respectively. A beam is incident at normal direction onto the antennas, with polarization along the longitudinal direction of the antennas. (b) The retrieved real part (black square) and imaginary part (red circle) of optical coupling constant between the two antennas, and the dissipations of the long (blue diamond) and short antennas (green triangle) as a function of their edge-to-edge separation s.

The coupling constant has an imaginary part (red circle) that is only slightly less than the dissipation of both antennas (blue diamond and green triangle) over a broad range of s up to about 250 nm. The approximate equity $\mathrm{Im}(\kappa_{12})^2 \approx \gamma_1\gamma_2$ indicates the presence of an anti-Hermitian term of rank 1 in the governing Hamiltonian of the plasmonic system; i.e., both antennas primarily couple to a single radiative decay channel. The slight difference between the anti-Hermitian coupling strength $\mathrm{Im}(\kappa_{12})$ and the dissipations at very small antenna separation is mainly due to the intrinsic Ohmic loss of the antennas. As s increases above 250 nm, the effect of other radiative channels, such as electric quadrupole and magnetic dipole radiation modes, starts to become significant, and the assumption of a single continuum channel no longer holds. Consequently, the imaginary part of the coupling constant deviates significantly from the dissipation rates of the antennas, and the foregoing analysis no longer applies in this regime.

At very small separations, the real (Hermitian) part of the coupling coefficient exhibits a large negative real part, which is dominated by the direct near-field coupling between the two antennas. With increasing distance, the near-field coupling decreases rapidly, and the real part of the coupling crosses zero at a separation around 30 nm, where the direct near-field coupling is canceled by the Cauchy principal value of the indirect coupling, leaving a purely anti-Hermitian coupling between the two antennas. As Fig. 1(b) shows, the imaginary part of the coupling constant is greater than the real parts for a broad antenna separation range from 20 nm to 350 nm. Thus, the coupled optical antennas serve as a model system for studying the interesting physics in a physical open system dominated by the anti-Hermitian coupling.

Next, we extend the plasmonic system to include five optical antennas with deep subwavelength spacing [Fig. 2(a)]. The length of the antennas ranges from 450 nm on one side to 610 nm on the other side with a step of 40 nm. The edge-to-edge spacing between the nearest neighboring antennas is 45 nm, and the separations between the second, third, and fourth nearest neighbors are 130, 215, and 300 nm, respectively. As indicated by Fig. 1(b), this configuration gives rise to complex coupling coefficients among the antennas that are dominated by their imaginary (anti-Hermitian) part. The anti-Hermitian part of the coupling constants roughly satisfies $\mathrm{Im}(\kappa_{pq})^2 \approx \gamma_p\gamma_q$ up to the third nearest neighbor ($s = 215$ nm), but not for the two antennas at the two ends (fourth nearest neighbor). However, as the two antennas at the two ends have dramatically different lengths and therefore very different resonance frequencies, this deviation has only a small effect on the overall performance.

In the simulation, a plane wave is incident at normal incidence onto the array of antennas. As shown in Fig. 2(b), each antenna exhibits a large resonance peak at approximately its uncoupled resonance frequency [Fig. 2(c)], where all the other antennas are strongly suppressed, leading to selective excitation of an individual antenna. This observation is consistent with the theoretical analysis given by Eq. (5), despite the presence of Hermitian coupling constants and Ohmic loss that result in a deviation of κ_{pq} from $i\gamma_p\gamma_q$ for interaction between certain antennas. In contrast to the selective excitation and sharp spectral features for the coupled antenna array, an array of uncoupled antenna exhibits very poor excitation selectivity due to the relative broad line width of the resonance peak, as shown in Fig. 2(c).

To visualize the selective excitation of individual antennas, we numerically obtained the out-of-plane electric field intensity distribution of the antenna array at the resonance frequencies of each antenna, as shown in Figs. 3(a)–3(e). Note that the out-of-plane component of the electric field is proportional to the surface charge distribution at the air-metal interface. The field distribution confirms that the antennas are individually excited at their resonance wavelengths, and the hot spots shifted from the shortest antenna at 1200 nm wavelength to the longest antenna at a wavelength of 1600 nm. Selective excitation among a plasmonic antenna array has been theoretically proposed previously [29], in which the radiative loss and coupling among the antennas are strongly suppressed by placing a ground plane underneath the antenna array. In contrast, the coupling

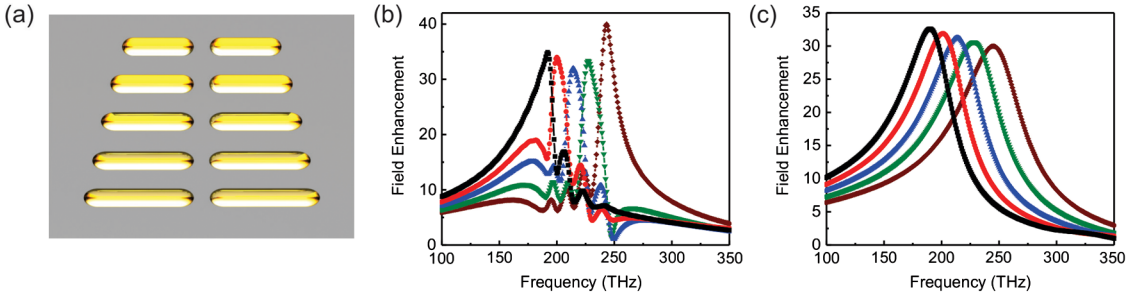

FIG. 2 (color online). Numerical simulations on an array of antennas with anti-Hermitian coupling showing selective excitation of individual antennas by a plane wave. (a) Schematic of a plasmonic antenna array consisting of five optical antennas with gradually varying lengths. (b) Calculated electric field magnitude at the gap center of each antenna versus the optical wavelength. (c) Spectral response for five uncoupled antennas with the same geometries as (a).

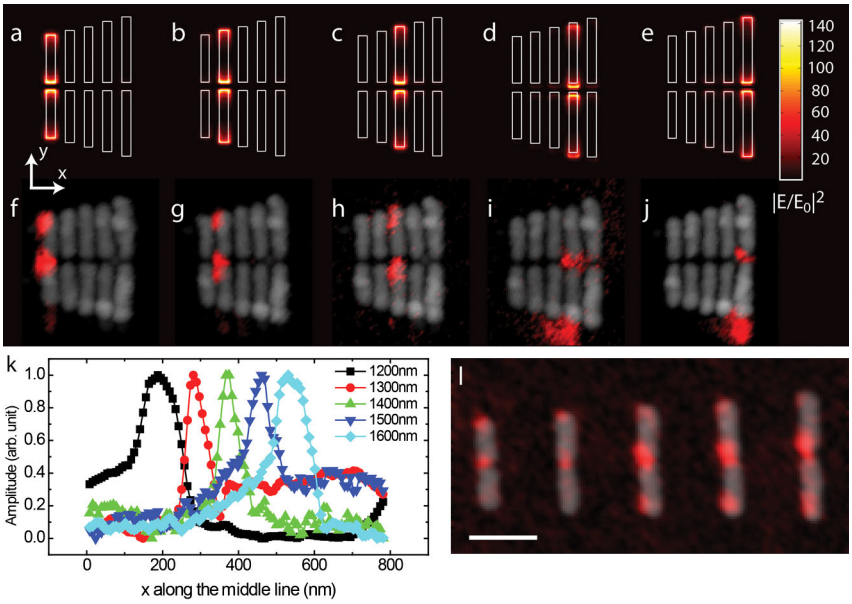

FIG. 3 (color online). Experimental verification of the selective excitation of individual antennas in the plasmonic antenna array. (a)–(e) Simulated near-field distributions of the antenna array at five different wavelengths: 1200 nm (250 THz), 1300 nm (230.8 THz), 1400 nm (214.3 THz), 1500 nm (200 THz), and 1600 nm (187.5 THz). (f)–(j) The corresponding experimental observations show very good agreement with the simulations. (k) Measured intensity of light integrated along the y direction, versus x, at each measured wavelength. (l) The near-field measurement at 1400 nm wavelength on the control sample, which consists of an array of antennas with the same geometry specification but at a large nearest neighbor separation of 300 nm.

mediated by radiation plays a key role in achieving the selective excitation in our work.

Experimentally, we fabricated the plasmonic antenna array and directly observed selective excitation of individual antennas at carefully chosen wavelengths, as shown in Fig. 3. Figures 3(f)–3(j) show the near-field optical distribution obtained by near-field scattering optical microscope (NSOM) for the array of optical antennas at five different wavelengths from 1200 nm to 1600 nm at a step of 100 nm. At each optical excitation wavelength, only a single antenna was strongly excited, which is in good agreement with the simulation results. Note that the asymmetric field distribution in the measurement may be caused by the asymmetric shape of the NSOM tip because of the degradation of the tip during the measurement. The NSOM measured localization of light in the antenna array is further quantified by a plot of intensity of light integrated along the y direction, versus x, at each measured wavelength, as shown in Fig. 3(k). On average, light is strongly confined within a scale of 70 nm along the x direction at each excited wavelength.

To highlight the role that the coupling among the antennas plays, a control sample that consists of an array of antennas with the same geometrical parameters, but spatially separated far (300 nm) from each other, was measured, at a wavelength of 1300 nm. At this separation, there exists a significant difference between the imaginary part of the coupling constant and the dissipation rate of each antenna, and therefore a single open channel approximation does not apply. As shown in Fig. 3(l), there is no selective excitation of individual antennas as several antennas were simultaneously excited. The comparison between the control sample and the well-designed antenna array implies that the coupling among antennas mediated by a single decay channel plays a significant role in achieving selective excitation of individual antennas.

While most studies on coupled plasmonic systems have focused on real coupling constants that primarily induce mode splitting [30–32], we show that coupling constants that are dominated by the imaginary part introduce the interesting functionality of light manipulation in the deep subwavelength scale. Nanomanipulation of optical hot spots has been realized by various means including time reversal, adaptively shaping the wave front and polarization of the incident beam [33–36], which, however, involves complicated temporal-spatial light modulation techniques. It has been shown numerically that a number of distinct patterns in an array of plasmonic particles could be excited by a plane wave; the method was based on a numerical searching process by varying all the possible incidence angles and wavelengths [37]. In contrast, we have employed a robust design method based on the anti-Hermitian coupling that is usually used to describe open quantum systems. It has also been experimentally demonstrated that in a linear array of plasmonic particles, the particles at the two ends can be selectively excited [38]. In contrast, our work represents a significant step forward by experimentally demonstrating the selective excitation of each individual element in the array.

The authors are grateful for financial support from the Multidisciplinary University Research Initiative (MURI) sponsored by the Air Force Office of Scientific Research (AFOSR) under Grant No. FA9550-12-1-0024. S. Z. acknowledges financial support from the European Commission under the Marie Curie Career Integration Program. S. Z., Z. Y., and Y. W. contributed equally to this work.

*To whom correspondence should be addressed.
xiang@berkeley.edu

[1] J. Okolowicz, M. Ploszajczak, and I. Rotter, Phys. Rep. **374**, 271 (2003).
[2] G. E. Makhmetov, A. G. Borisov, D. Teilletbilly, and J. P. Gauyacq, Europhys. Lett. **27**, 247 (1994).
[3] Y. Alhassid, Rev. Mod. Phys. **72**, 895 (2000).
[4] R. H. Dicke, Phys. Rev. **93**, 99 (1954).
[5] P. Bartsch *et al.*, Eur. Phys. J. A **4**, 209 (1999).
[6] R. Bertini *et al.*, Phys. Lett. B **90**, 375 (1980).
[7] R. Bertini *et al.*, Phys. Lett. B **136**, 29 (1984).
[8] H. Feshbach, Ann. Phys. (N.Y.) **19**, 287 (1962).
[9] N. Auerbach and V. Zelevinsky, Rep. Prog. Phys. **74**, 106301 (2011).
[10] I. Rotter, Rep. Prog. Phys. **54**, 635 (1991).
[11] N. Auerbach, V. Zelevinsky, and A. Volya, Phys. Lett. B **590**, 45 (2004).
[12] A. A. Svidzinsky and J. T. Chang, Phys. Rev. A **77**, 043833 (2008).
[13] R. Röhlsberger, K. Schlage, B. Sahoo, S. Couet, and R. Rüffer, Science **328**, 1248 (2010).
[14] M. O. Scully, Phys. Rev. Lett. **102**, 143601 (2009).
[15] E. Prodan, C. Radloff, N. J. Halas, and P. Nordlander, Science **302**, 419 (2003).
[16] S. Zhang, D. A. Genov, Y. Wang, M. Liu, and X. Zhang, Phys. Rev. Lett. **101**, 047401 (2008).
[17] N. Liu, L. Langguth, T. Weiss, J. Kästel, M. Fleischhauer, T. Pfau, and H. Giessen, Nature Mater. **8**, 758 (2009).
[18] N. Verellen, Y. Sonnefraud, H. Sobhani, F. Hao, V. V. Moshchalkov, P. Van Dorpe, P. Nordlander, and S. A. Maier, Nano Lett. **9**, 1663 (2009).
[19] F. Hao, Y. Sonnefraud, P. Van Dorpe, S. A. Maier, N. J. Halas, and P. Nordlander, Nano Lett. **8**, 3983 (2008).
[20] B. Luk'yanchuk, N. I. Zheludev, S. A. Maier, N. J. Halas, P. Nordlander, H. Giessen, and C. T. Chong, Nature Mater. **9**, 707 (2010).
[21] J. A. Fan, C. Wu, K. Bao, J. Bao, R. Bardhan, N. J. Halas, V. N. Manoharan, P. Nordlander, G. Shvets, and F. Capasso, Science **328**, 1135 (2010).
[22] N. Liu, M. Hentschel, Th. Weiss, A. P. Alivisatos, and H. Giessen, Science **332**, 1407 (2011).
[23] S. Zhang, D. A. Genov, Y. Wang, M. Liu, and X. Zhang, Phys. Rev. Lett. **101**, 047401 (2008).
[24] N. Liu, L. Langguth, T. Weiss, J. Kästel, M. Fleischhauer, T. Pfau, and H. Giessen, Nature Mater. **8**, 758 (2009).
[25] L. Verslegers, Z. Yu, Z. Ruan, P. B. Catrysse, and S. Fan, Phys. Rev. Lett. **108**, 083902 (2012).
[26] R. Taubert, M. Hentschel, J. Kästel, and Harald Giessen, Nano Lett. **12**, 1367 (2012).
[27] P. Muhlschlegel, H. J. Eisler, O. J. F. Martin, B. Hecht, and D. W. Pohl, Science **308**, 1607 (2005).
[28] See Supplemental Material at http://link.aps.org/supplemental/10.1103/PhysRevLett.109.193902 for detailed information.
[29] G. Lévêque and O. J. F. Martin, Phys. Rev. Lett. **100**, 117402 (2008).
[30] H. Wang, D. W. Brandl, F. Le, P. Nordlander, and N. J. Halas, Nano Lett. **6**, 827 (2006).
[31] H. Liu, D. Genov, D. Wu, Y. Liu, Z. Liu, C. Sun, S. Zhu, and X. Zhang, Phys. Rev. B **76**, 073101 (2007).
[32] N. Liu, H. Liu, S. N. Zhu, and H. Giessen, Nature Photon. **3**, 157 (2009).
[33] M. Aeschlimann, M. Bauer, D. Bayer, T. Brixner, F. J. García de Abajo, W. Pfeiffer, M. Rohmer, C. Spindler, and F. Steeb, Nature (London) **446**, 301 (2007).
[34] A. Kubo, K. Onda, H. Petek, Z. Sun, Y. S. Jung, and H. K. Kim, Nano Lett. **5**, 1123 (2005).
[35] X. Li and M. I. Stockman, Phys. Rev. B **77**, 195109 (2008).
[36] G. Volpe, S. Cherukulappurath, R. J. Parramon, G. Molina-Terriza, and R. Quidant, Nano Lett. **9**, 3608 (2009).
[37] A. F. Koenderink, J. V. Hernández, F. Robicheaux, L. D. Noordam, and A. Polman, Nano Lett. **7**, 745 (2007).
[38] R. de Waele, A. F. Koenderink, and A. Polman, Nano Lett. **7**, 2004 (2007).